3.1 Determination of the Material Properties of Road Pavement Component Layers from Surface Deflection Measurements – Development of Mathematical Model and Software

A mathematical model for the determination of stresses, strains and displacements for given surface loads, at any point in a multi-layered pavement system, has been formulated. This model simplifies the problem considerably and the algebra in the numerical scheme is lesser than in the models of multi-layered systems available in the literature. Transfer matrix approach is used in representing the interface conditions which further simplifies the problem. A numerical scheme and a software package have been developed for the above problem and validated against results published in the literature. Furthermore, the surface displacement given by the model is compared with experimental results obtained at CRRI with a falling weight deflectometer (FWD). The comparison of model results of average scaled deflection, for different values of radial distance from the loading point, with the FWD results for a three-layered system are shown in *Figs. 3.1.1* and *3.1.2* for two test points; the three-layered system consists of a top layer of bituminous macadam, a middle layer of stabilized soil and a subgrade of infinite thickness.

It can be seen from the *Figs. 3.1.1* and *3.1.2* that the vertical displacements obtained using the model are slightly higher than the FWD results. The reason for this is the sensitivity of the problem to the material properties of the layered system; the material properties used in the analysis are those that have been obtained using the backward analysis for deflection values obtained with FWD. The question whether a choice of values of elastic properties, other than those given by FWD, improves the agreement between the model and the experimental results is being investigated. Presently, the problem is being analyzed for a wide range of elastic modulii values typical of Indian roads which might give more insight into the problem. Though the results given here are only deflection values for a maximum of three layers, the numerical scheme and the software can be used to obtain the values of stresses, strains and displacements at any point in a *n*-layered medium for both the uniformly distributed and concentrated surface loads.

(Sridevi Jade, P.K.Nanda and S.P.Pokhriyal* (*CRRI))*

3.2 Analysis of Strength and Deformation of Jointed Rocks

Two aspects of the jointed rock mass behavior is dealt with here: the finite element modeling of jointed rock mass as an equivalent continuum and the comparison of empirical strength criteria of jointed rock mass. In the finite element modeling, the jointed rock properties are

Fig. 3.1.1. Average scaled deflection at test point 1 in a three-layer pavement.

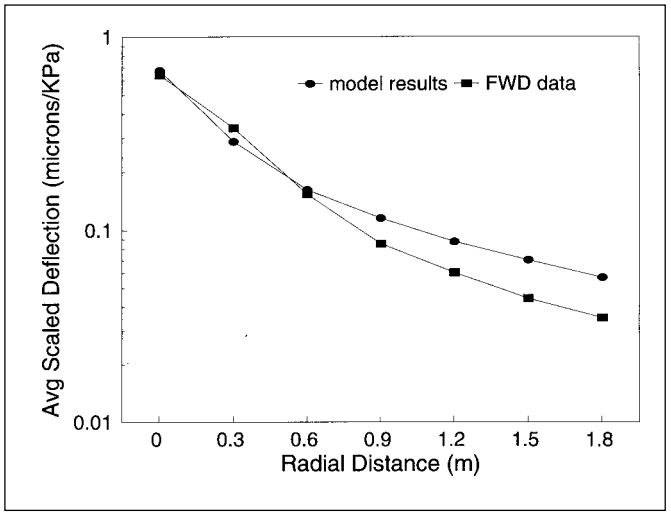

Fig. 3.1.2. Average scaled deflection at test point 2 in a three layer pavement.

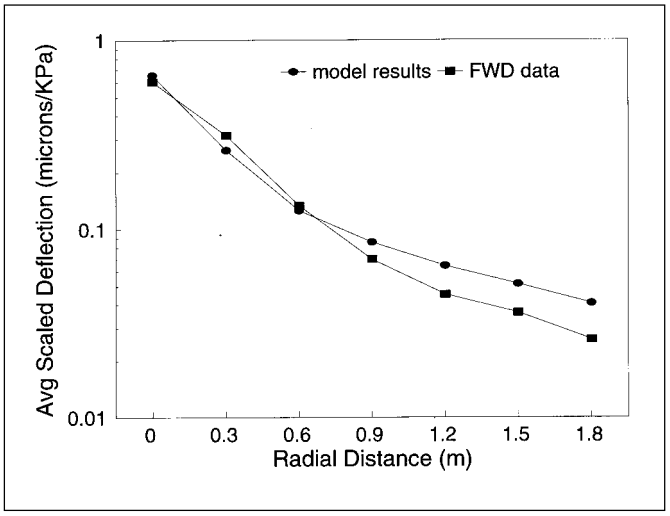

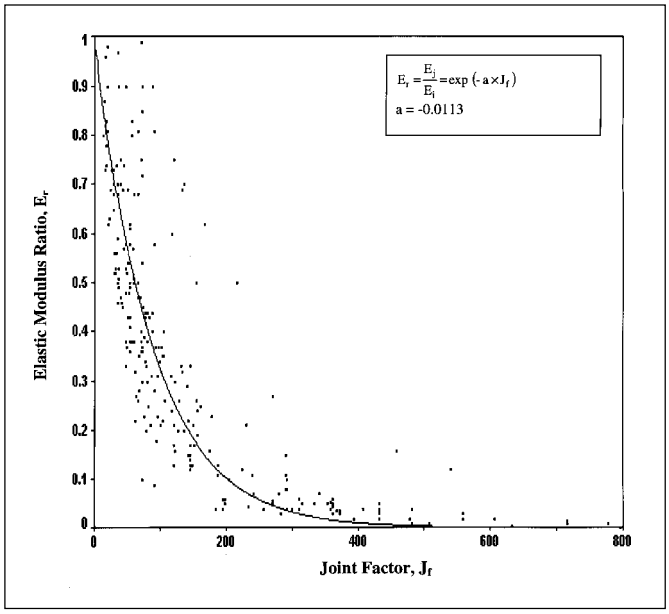

Fig. 3.2.1. Plot of unconfined compressive test data with the relationship fitted for E_r.

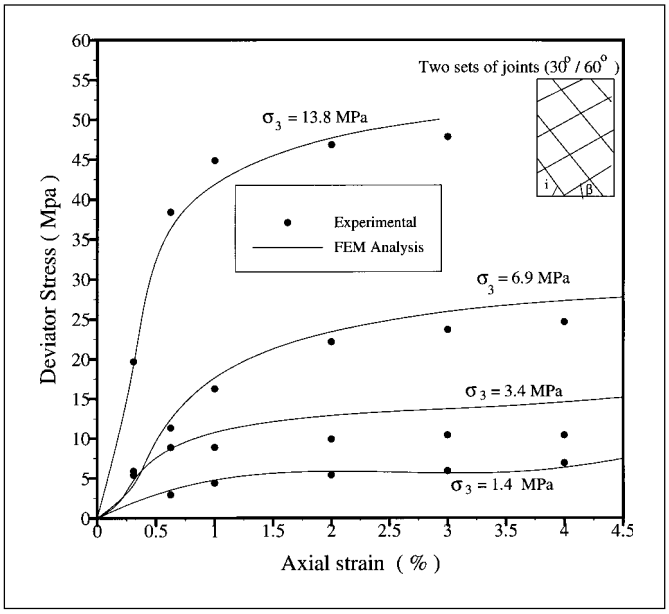

Fig. 3.2.2. Stress-strain plot for a block jointed specimen of Gypsum Plaster.

represented by a set of empirical relationships which express the properties of the jointed medium as a function of joint factor (J_f) and properties of the intact rock. These relationships have been arrived at from a large set of experimental data of tangent elastic modulus. The empirical relationship fitted from the experimental data for tangent modulus ratio E_r is given in *Fig. 3.2.1*; E_r is the ratio of the tangent modulus of the jointed rock to the intact rock.

Results have been presented in the form of stress-strain curves for jointed rocks *(Fig. 3.2.2)* and compared with available experimental results. It can be seen from the stress-strain curves that equivalent continuum analysis gives best results for both single and multiple jointed rocks. The reliability of the analysis depends upon the estimation of J_f which is a function of the joint orientation, joint frequency and joint strength.

The empirical strength criteria for the jointed rocks given by Hoek and Brown, Yudhbir et al., Ramamurthy and Arora, and Mohr-Coulomb have been incorporated in the nonlinear finite element analysis of jointed rock using equivalent continuum approach to determine the failure stress. The results have been presented in the form of major principal stress (Failure stress, σ_1) versus minor principal stress (Confining pressure, σ_3) at failure *(Fig. 3.2.3),* obtained using different failure criteria and compared with the available experimental results. The major principal stress at failure obtained using

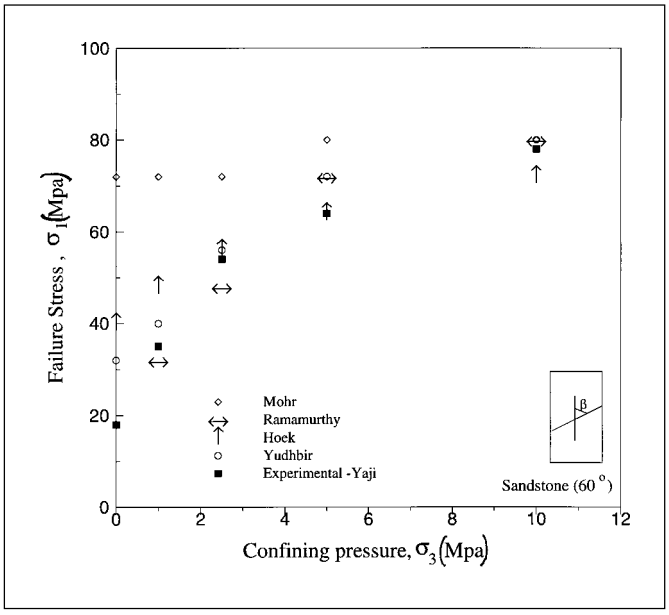

Fig. 3.2.3. Comparison of strength criteria for single jointed specimen of Sandstone.

Ramamurthy and Arora's criteria compares very well with the experimental results.

(Sridevi Jade and T.G.Sitharam (*IISc))*

3.3 Finite Element Analysis of Discontinuities in the Rock Mass

Nonlinear finite element analysis of jointed rock has been carried out by representing the joints explicitly to study the mechanical behavior of discontinuities in rock masses.

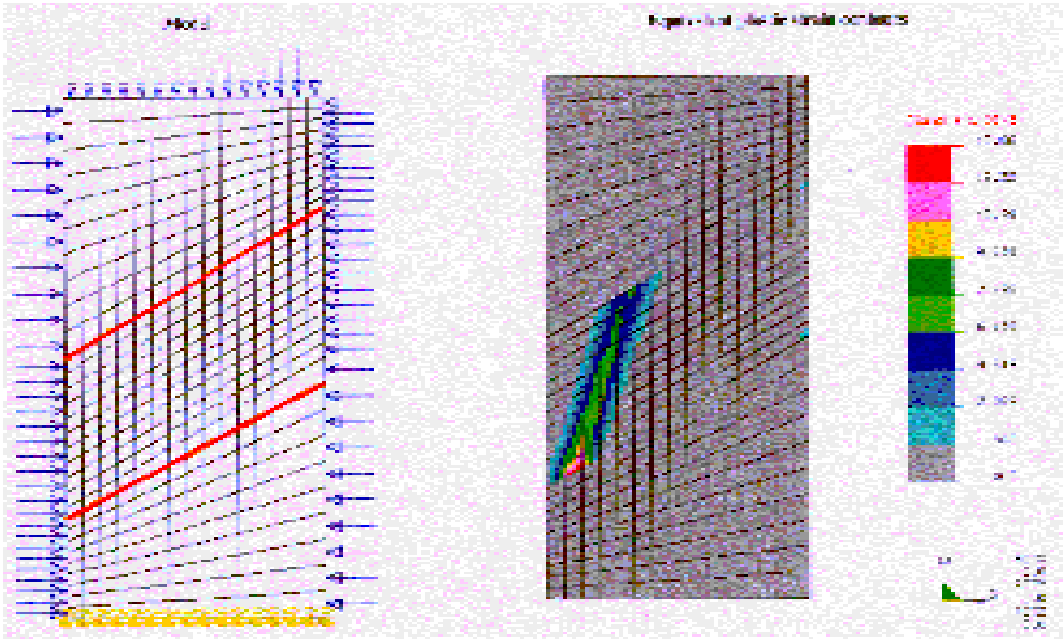

Fig. 3.3.1. FEM model and the equivalent plastic strain contours with single discontinuity.

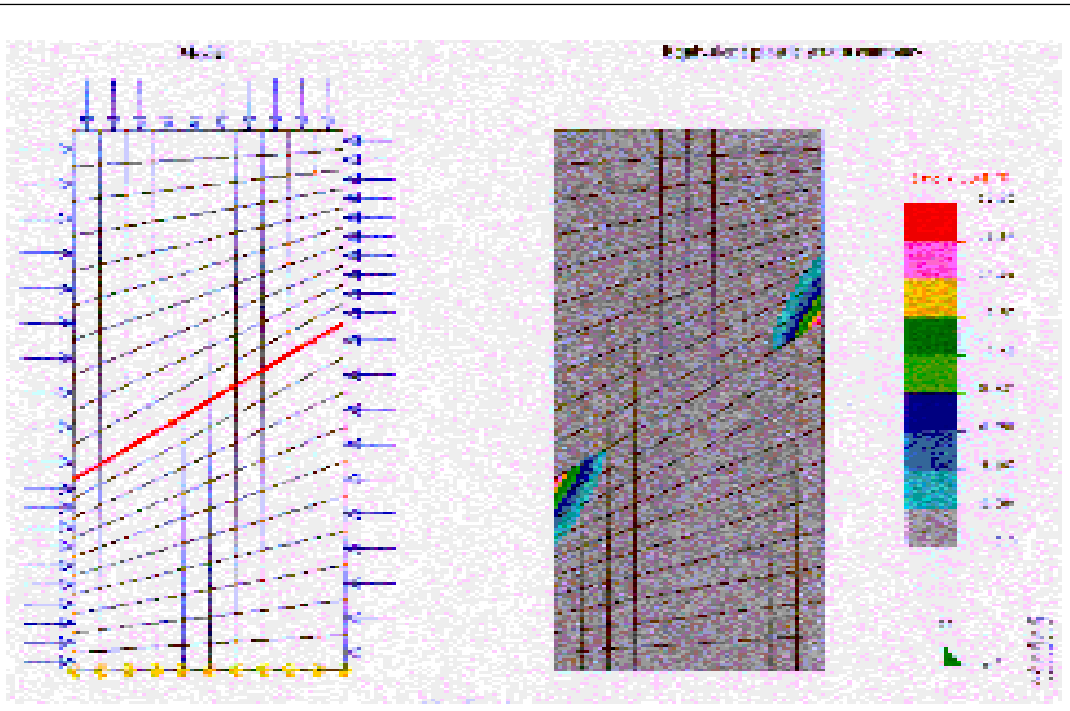

Fig. 3.3.2. FEM model and the equivalent plastic strain contours with two discontinuities.

Three different rock materials have been analyzed with single and multiple joints for different confining pressures and axial loads. Intact rock mass is modeled using 2-D Plane strain elements and the joint is explicitly modeled using 2-D Gap and Friction elements. The model is subjected to uniform confining pressure on the two vertical sides and uniform axial stress on the top. Isotropic elasto-plastic material behavior with no strain softening is used

in the analysis. The axial load is applied in series of steps or increments. The incremental solution is performed in a step-by-step manner until the full-specified loads are applied. In each increment the modified Newton-Raphson iterative scheme is performed until convergence is achieved. Mohr-Coulomb yield criterion is used in the analysis to determine the major principal stresses at failure. The inclination of the discontinuity with the major principal stress direction is varied from 0 to 90 degrees and the confining pressure is varied from 0 to 10 MPa. Sensitivity analysis of the model is carried out for coefficients of friction and normal and tangential stiffnesses at the interface.

The finite element model along with the equivalent plastic strain contours are given in *Figs. 3.3.1* and *3.3.2* for the one and two discontinuities respectively. The rock mass is said to have failed when the yield criterion for the elastic behavior is reached and the rock mass behavior becomes plastic. The equivalent plastic strain contours represent the weak zone in the rock mass where the rock starts to fail. It can be seen from *Figs. 3.3.1* and *3.3.2* that the failure occurs at the discontinuity for the case of the single joint. For two joints, the failure occurs in the region between the two discontinuities, a weak zone. The strength of the FEM technique in the above lies in its generality and flexibility to handle all types of loads, sequences of construction, support conditions and different material properties.

(Sridevi Jade and H.M.Chandrashekhar)

3.4 Non-Newtonian Fluid Flow Simulation

Non-Newtonian viscoelastic fluids have a complex rheological behaviour. The provocative flow phenomena observed with polymeric fluids cannot be predicted by the Navier-Stokes equations. The theoretical challenge is to model the complex rheological behaviour of polymeric fluids in suitable constitutive equations and to use these models in computations. Flow elasticity is characterised by the Weissenberg number, *We*, defined as the ratio of a characteristic fluid relaxation time to a characteristic flow time. Viscoelastic flow computation at high *We* remains a difficult task even today. The upper convected Maxwell (UCM) and the Oldroyd B models of viscoelasticity are employed to investigate flow in the entrance region of a channel. The objective of the investigation has been to study the development of viscoelastic stresses near the entrance region as *We* is increased, to better understand the high *We* problem. A finite volume approach is adopted to discretise the governing equations on a computational grid, and the continuity equation is treated by a pressure based method. Results for *We* of 0.1 for the UCM model, and upto *We* of 10 for the Oldroyd B model have been discussed. Viscoelastic flow around a cylinder in an unbounded flow and placed in a channel is also being investigated. Models which consider all polymer chains in terms of mechanical equivalents, irrespective of their chemical structure, are incapable of explaining many unusual rheological phenomena. An energetically crosslinked transient network (ECTN) model has been recently given in the literature in which a polymer solution is assumed to contain a physical crosslink and an energetic crosslink. Investigation of flow around an array of cylinders using the ECTN model is also under progress.

(A. Kumar, Hema Ravi, R.A. Mashelkar (*CSIR Hq.))*

3.5 Supersymmetric Finite-Difference Formulae

New finite-difference formulae have been developed such that the discretisation of the Laplace operator is rotationally invariant. These formulae, referred to as supersymmetric finite-difference formulae, ensure that the mean value theorem for a harmonic function is preserved on the discretisation of the Laplace equation. Formulae in two and three dimensions have been obtained. Supersymmetric discretisation of the Laplacian in n-dimensions is given.

The l_2 and l_∞ stability limits of the heat conduction equation in n-dimensions, which are 1/2n in conventional differencing, have been shown to be 1/2 and $2^{n-2}/(2^n-1)$, respectively, under the supersymmetric discretisation. Thus while the l_2 stability limit for the supersymmetric discretisation is dimension-independent, the l_∞ stability limit is greater than 1/4 for any n.

(A. Kumar)

3.6 Numerical Investigation of Flow Around a Vented Sphere

Several attempts comprising passive and energetic methods have been made in the past to control the flow past bluff bodies in order to achieve drag reduction. While most of these pertain to two-dimensional bluff bodies, there have been only a few attempts on a sphere, which represents an idealised three-dimensional bluff body. When the stagnation and the base regions of a sphere are interconnected through an internal duct, mass, momentum and energy are passively added into the near-

wake. The above concept of natural ventilation to reduce the pressure drag of a sphere has been proposed earlier by others and experimently investigated. We have investigated this interesting flow using Navier-Stokes equations. Axisymmetry of the flow has been assumed, and a k-ε turbulence model has been used. An attempt has been made to gain insight into the mechanics of the flow. Interesting interactions between the external shear layer and the vent-jet were reported. Features of the near-wake flow leading to some understanding of the vortex shedding at a subcritical Reynolds member have been observed.

(A. Kumar and G.K. Suryanarayana (*NAL))*

3.7 Multi-Storey Infilled Frames Under Combined Lateral and Vertical Loading

Infilled frames have been a subject of immense interest for the researchers for well over three decades as an efficient and effective lateral load resisting system. Linear finite element analysis has been carried out on 4-storey reinforced concrete (R.C.) infilled frame infilled with brick

Table 3.7

Reduction of deformations and associated moments and forces in infilled frames over conventional frames

		% reduction in the function over its conventional frame counterpart	
Structural Function	**Load case**	**Full contact**	**Separation**
Lateral deformation	i. lateral load only	89.10 - 99.98	87.47 - 99.97
	ii. combined loads	89.08 - 99.98	88.35 - 99.97
	iii. vertical load only	85.58 - 99.95	83.04 - 99.95
Vertical deformation	i. lateral load only	23.94 - 98.97	25.48 - 98.90
	ii. combined loads	45.80 - 99.90	45.10 - 99.89
	iii. vertical load only	57.84 - 99.82	56.41 - 99.82
Bending moments			
a. l floor beam	i. lateral load only	94.87 - 99.98	91.35 - 100.26
	ii. combined loads	93.64 - 99.94	90.59 - 99.91
	iii. vertical load only	90.69 - 99.91	89.19 - 99.89
b. Windward Column	i. lateral load only	90.90 - 99.66	89.92 - 99.27
	ii. combined loads	92.14 - 99.69	92.63 - 99.69
	iii. vertical load only	85.63 - 99.79	78.15 - 99.83
c. Leeward Column	i. lateral load only	89.70 - 99.87	83.27 - 99.87
	ii. combined loads	88.73 - 99.70	87.67 - 99.73
	iii. vertical load only	85.63 - 99.79	78.15 - 99.83
Shear force			
l floor beam	i. lateral load only	83.20 - 97.42	67.30 - 96.02
	ii. combined loads	78.24 - 97.32	67.88 - 97.24
	iii. vertical load only	76.30 - 97.19	69.62 - 97.14
Axial Force			
a. Windward Column	i. lateral load only	-147.35 - 163.36	-143.50 -179.58
	ii. combined loads	55.25 - 93.99	55.22 - 94.26
	iii. vertical load only	37.88 - 91.12	38.66 - 91.14
b. Leeward Column	i. lateral load only	9.84 - 79.60	6.05 - 75.98
	ii. combined loads	23.93 - 88.37	25.42 - 89.00
	iii. vertical load only	42.69 - 88.81	42.46 - 81.79

(- sign indicates increase)

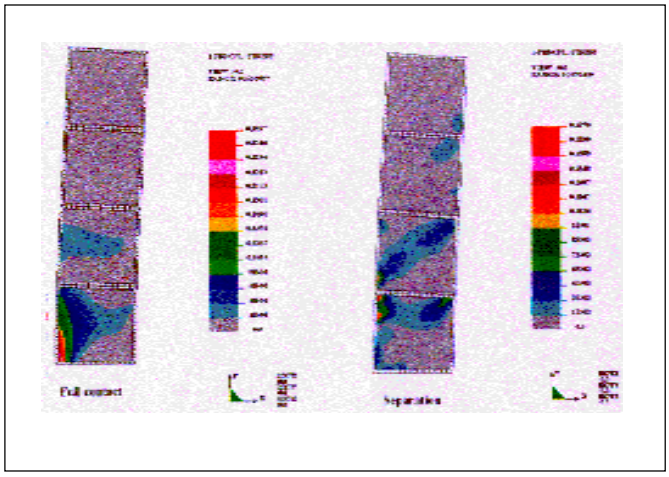

Fig. 3.7.1. Principal tensile stress contours in an infilled frame under combined lateral and vertical loading.

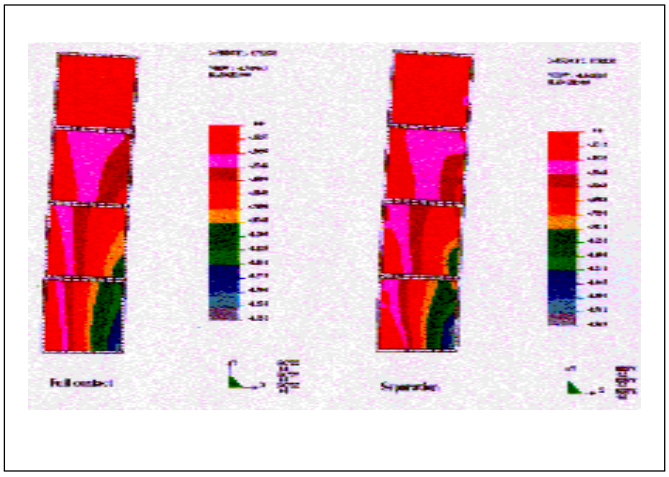

Fig. 3.7.2. Principal compressive stress contours in an infilled frame under combined lateral and vertical loading.

masonry under constant lateral loads and varying vertical loads. Varying relative stiffnesses of the frame to infill and varying spans are the parameters considered in the analysis for two cases of contact at interface, *viz.* full contact and separation.

The finite element modeling consists of 2-D plane stress elements representing the infill and 3-D beam elements for the bounding frame. Short and very stiff 3-D beam elements are used as links to represent the interface wherein the node connecting the R.C. frame is merged with the node on the frame and, for the node at the masonry end of the inplane, rotational degree of freedom is suppressed so that no moment is transferred to the masonry. The physical separation of the frame from the masonry is simulated using an iterative scheme where, after each run, the axial force in each link is checked and, if found in tension, the link removed. This iteration is continued till a stable configuration of separations are reached.

Four relative stiffness values and three aspect ratios have been considered in the analysis which are illustrated in the sketch on the right.

Conventional frames without the masonry have also been analysed for the same conditions of geometry and loading. The loading consists of 25 kN as the nodal lateral load at the beam level and the transverse loads due to the live component is varied from 10 kN/m to 40 kN/m on each floor beam. For the case of vertical loads acting alone, a load of 30 kN/m has been considered.

Typical stress contours and deformed geometry have been presented in *Figs. 3.7.1* and *3.7.2* and a typical graphical picture of variation of bending moments have been presented in *Fig. 3.7.3*. Substantial reduction in lateral and transverse deformations, bending moments, shear forces and axial forces are observed in infilled frames and in its members in comparison to conventional frames which are illustrated in *Table 3.7*.

The masonry stresses (*Fig 3.7.1* and *Fig 3.7.2*), which are highly concentrated in the ground floor wall panel are in for favourable change under combined loads. The principal tensile stresses tend to reduce substantially under combined loads in comparison to those in the case of lateral loads acting alone. The principal compressive stresses tend to increase with the addition of vertical loads. The maximum stresses are normally located at the ends of the leading and trailing diagonals of the ground floor panel thus substantiating the diagonal strut theory even for multistorey frames. The width of the diagonal strut does

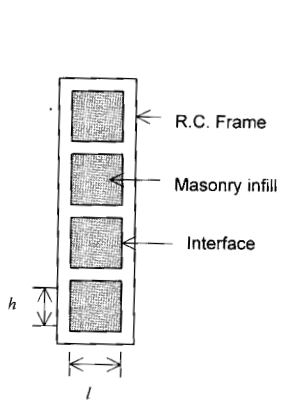

DETAILS OF GEOMETRY

Relative Stiffness	Beam/Column sizes (mm)
3.52	400x400
7.04	200x200
11.85	200x100
14.70	200x75

h (mm)	*l* (mm)	aspect ratio
2700	2700	1.0
2700	4050	1.5
2700	5400	2.0

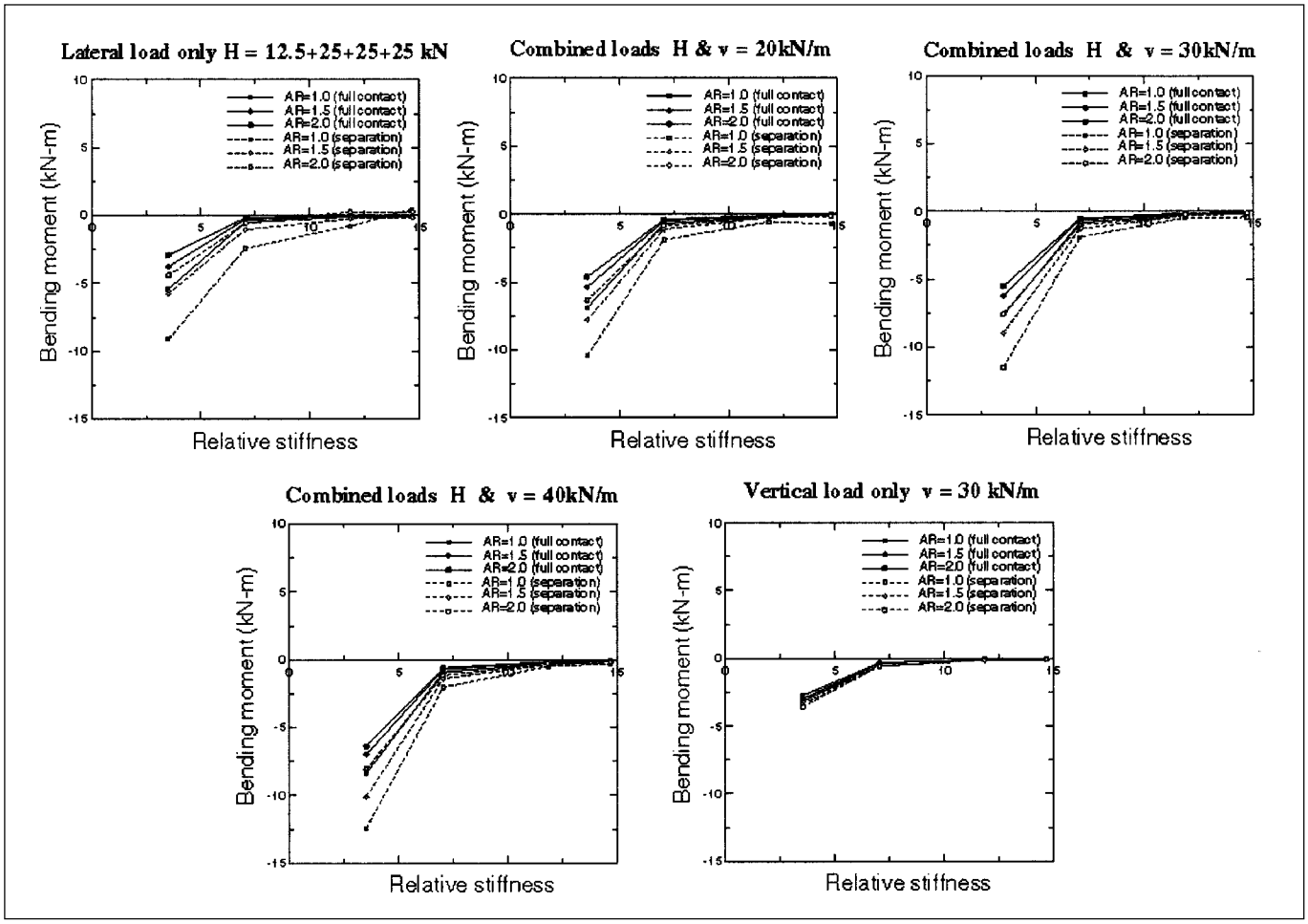

Fig. 3.7.3. Variation of maximum bending moment in I-floor beam of 4-storey infilled frame for different load cases.

have a positive influence due to the vertical load component.

Finally, vertical loads, which act in tandem with lateral loads, do have a favourable influence on the behaviour of multistorey infilled frames. The change in stiffness characteristics is not very significant in contrast to strength characteristics. Frames with solid infill are very efficient and effective to stand upto the lateral effects of wind and seismic activity. Further work is underway to include the effects of still floors (wall-less ground floors for parking or other amenities) and lack of surface contact between the floor beams and the masonry walls below.

(Sridevi Jade, D.S. Prakash and R. Jagdish**
*(*Bangalore University))*